Available online at www.sciencedirect.com
SCIENCE DIRECT
Journal of Solid State Chemistry 179 (2006) 1100–1109
JOURNAL OF SOLID STATE CHEMISTRY
www.elsevier.com/locate/jssc

Synthesis and phase transition of Li–Mn–O spinels with high Li/Mn ratio by thermo-decomposition of $LiMnC_2O_4(Ac)$

Xin-Cun Tang[a,b,*], Cheng-Kui Jiang[a], Chun-Yue Pan[a], Bo-Yun Huang[b], Yue-Hui He[b]

[a]College of Chemistry & Chemical Engineering, Central South University, Changsha, Hunan 410083, PR China
[b]State Key Laboratory of Powder Metallurgy, Central South University, Changsha, Hunan 410083, PR China

Received 26 April 2005; received in revised form 20 October 2005; accepted 30 December 2005
Available online 7 February 2006

Abstract

$LiMnC_2O_4(Ac)$ precursor in which Li^+ and Mn^{2+} were amalgamated in one molecule was prepared by solid-state reaction at room-temperature using manganese acetate, lithium hydroxide and oxalic acid as raw materials. By thermo-decomposition of $LiMnC_2O_4(Ac)$ at various temperatures, a series of $Li_{1+y}[Mn_{2-x}Li_x]_{16d}O_4$ spinels were prepared with Li_2MnO_3 as impurities. The structure and phase transition of these spinels were investigated by XRD, TG/DTA, average oxidation state of Mn and cyclic voltammeric techniques. Results revealed that the Li–Mn–O spinels with high Li/Mn ratio were unstable at high temperature, and the phase transition was associated with the transfer of Li^+ from octahedral 16*c* sites to 16*d* sites. With the sintering temperature increasing from 450 to 850 °C, the phase structure varied from lithiated-spinel $Li_2Mn_2O_4$ to $Li_4Mn_5O_{12}$-like to $LiMn_2O_4$-like and finally to rock-salt $LiMnO_2$-like. A way of determining x with average oxidation state of Mn and the content of Li_2MnO_3 was also demonstrated.

Keywords: Lithium manganese oxide; Phase transition; $LiMnC_2O_4(Ac)$; Room-temperature solid-state reaction; Lithium-ion batteries

1. Introduction

Lithium manganese oxides are the most attractive cathode materials for rechargeable lithium-ion batteries because of their low-cost and less toxicity compared to either cobaltates or nickelates [1]. Among these oxides, the spinel-framework compounds have been widely investigated due to scientific and commercial interest. As shown in Fig. 1, the interstitial spaces in the cubic close-packed array of oxygen for $LiMn_2O_4$ spinel provide a network of tetrahedral 8*a* sites, octahedral 16*c* and 16*d* sites. In the ideal spinel $LiMn_2O_4$, Li and Mn, respectively, occupy tetrahedral 8*a* and octahedral 16*d* sites with space group *Fd*3*m*; and the Li intercalate or deintercalate reversibly from 8*a* sites, which offers a theoretical capacity of 148 mA h/g with two charge/discharge plateaus at ca. 3.95 and 4.15 V (vs. Li^+/Li) [2]. However, the poor rechargeability restricts its commercial applications. A number of studies have been done to improve its rechargeability, for example, by replacing Mn with other alloying elements [3–5]. In particular, $Li[Mn_{2-x}Li_x]_{16d}O_4$, by partially replacing Mn with Li, have given rise to wide interests [6–8].

It is known that Li not only can substitute partially Mn in the octahedral 16*d* sites to form the manganese-absent spinels $Li[Mn_{2-x}Li_x]_{16d}O_4$ ($0 \leqslant x \leqslant 0.33$) but also can further occupy the octahedral 16*c* sites to form the lithium-rich spinels $Li_{1+y}Mn_2O_4$ ($0 \leqslant y \leqslant 1$) by resulting tetragonal structure up to the composition $Li_2Mn_2O_4$ ($y = 1$) [2]. As a result, a series of spinel $Li_{1+x+y}Mn_{2-x}O_4$ ($3x - 1 \leqslant y \leqslant 1 + 2x$) compounds are given in the Li–Mn–O phase diagram with the average valent of Mn varied from +3 to +4 [1,9,10]. For examples, at $x = 0$ and $y = 1$, the stoichiometric compound is the lithiated-spinel $Li_2Mn_2O_4$ in which all Mn are trivalent, it exhibits three voltage plateaus during the Li^+ intercalation/deintercalation,

*Corresponding author. College of Chemistry & Chemical Engineering, Central South University, Changsha, Hunan 410083, PR China.
Fax: +86 731 887 9616.
E-mail address: tangxincun@163.com (X.-C. Tang).

0022-4596/$ - see front matter © 2006 Elsevier Inc. All rights reserved.
doi:10.1016/j.jssc.2005.12.039

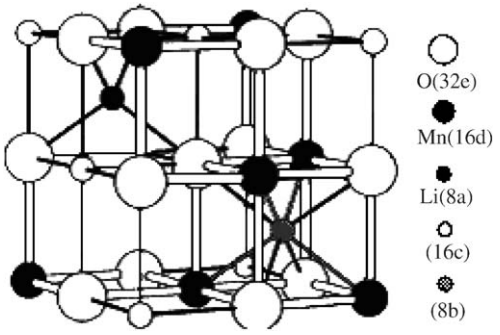

Fig. 1. The schematic drawing of the interstitial sites in the cubic close-packed array of oxygen for $LiMn_2O_4$ spinel.

respectively, in ca. 3.0, 3.95 and 4.15 V [6,11]; And at $x = 0.33$ and $y = 0$, the stoichiometric compound is given as $Li_4Mn_5O_{12}$ in which all Mn are tetravalent; it offers a theoretical capacity of 163 mA h/g in 3 V region and no capacity in the 4 V region [12–14]. From a structural point of view, when oxidation state of Mn falls below 3.5, the Jahn–Teller distortion occurs and consequently deteriorates the rechargeability of spinel compounds. Thus, the spinels $Li_{1+x+y}Mn_{2-x}O_4$ with high values of x and low values of y (e.g., $Li_4Mn_5O_{12}$) have been adapted to increase the average valence of Mn and further to improve the rechargeability. However, as suggested previously by various authors [7,12,14,15], the spinels $Li_{1+x+y}Mn_{2-x}O_4$ with high values of x are less thermo-stable than those with lower values of x at higher sintering temperature. This makes it difficult to be prepared by the direct solid-state reaction. For this purpose, the low-temperature preparation techniques were generally adopted such as hydrothermal method [14], etc. Moreover, as similar to Li–Mn–O spinels with the low Li/Mn ratio (~0.5), which the structure and electrochemical properties vary from sample to sample, the Li–Mn–O spinels with the high Li/Mn ratio also suffer from the same problem. For Li–Mn–O spinels with the low Li/Mn ratio, Xia et al. [16] and Yonemura et al. [17] considered that the oxygen stoichiometry was the key factor in determining the difference of the electrochemical properties of the $LiMn_2O_4$ samples prepared at different conditions. In this study, a novel idea has been provided to synthesize the unstable or meta-stable spinels $Li_{1+x+y}Mn_{2-x}O_4$ by designing a 1:1 Li/Mn ratio precursor $LiMnC_2O_4$(Ac). Because Mn^{2+} and Li^+ are amalgamated in one precursor molecule, this precursor lends itself to forming lithiated-spinel $Li_2Mn_2O_4$ when the organic elements (C and H) are decomposed by the heat treatment. Based on the lithiated-spinel $Li_2Mn_2O_4$, the phase transition of the $Li_{1+x+y}Mn_{2-x}O_4$ spinel series with high Li/Mn ratio has been further investigated. It indicates that the transfer of Li from 16*c* site to 16*d* site is one of the key factors in determining the properties and phase transition of the $Li_{1+x+y}Mn_{2-x}O_4$ spinel series with high Li/Mn ratio.

2. Experimental

2.1. Synthesis of precursor $LiMnC_2O_4$(Ac)

$LiMnC_2O_4$(Ac) precursor was synthesized by the method of the room-temperature solid-state reaction [18,19]. First, LiOH and oxalic acid were mixed in a molar ratio of 1:1 and ground in agate mortar until the mixture became sticky. Then, manganese acetate (in solid state) was added to the sticky mixture with the same molar amount, and ground for ab. 30 min. In this process, the vinegar odor could be smelt. The obtained materials were further dried to remove the water and acetic acid adsorbed on the product, and finally the xerogel $LiMnC_2O_4$(Ac) precursor was obtained.

2.2. Preparation of lithium manganese oxide

The lithium manganese oxides were prepared by sintering the $LiMnC_2O_4$(Ac) precursor in air at different temperatures for 12 h with the heating rate of 10 °C/min, without intermediate regrinding or other heating treatments.

2.3. Measurements and characterizations on the precursors and Li–Mn–O spinels

The elemental analysis and IR spectrum of the precursors were respectively performed on PE-2400C model elemental analyzer and Bio-RAD FTS-40 IR spectrometer (KBr disc). Before being determined, all samples of the precursors were dried at 120 °C in vacuum for 24 h. The thermogravimetry (TG) and differential thermal analysis (DTA) curves of $LiMn(C_2O_4)$(Ac) were recorded on a PE-DTA/1700 thermal analyzer with a heating rate of 10 °C/min. Powder X-ray powder diffraction patterns were recorded with a Rigaku D/Max-3B X-ray diffractometer, Cu/$K\alpha$. Scanning electron microscopy (SEM) and TEM micrographs were respectively obtained by using JSM-5600LV scanning electron microscope and HITACHI H-800 transmission electron microscope. Average oxidation state of Mn in the Li–Mn–O spinel products was determined by the redox titration with oxalic acid as reducing agent and the hot sulfuric acid as solvent of Li–Mn–O spinel, and the excess oxalate acid was back-titrated by potassium permanganate solution. Cyclic voltammetric (CV) curves of Li–Mn–O spinels were recorded on the CHI660 Electrochemical Workstation with the scan rate of 0.02 mV/s by using the powder microelectrode (PME) as working-electrodes. PMEs used in this work were made from Pt micro-disk electrodes of 0.1 mm in diameter. Pt micro-disk electrode was first chemically etched to form a cavity of tens of micrometers deep and then the cavity was filled with Li–Mn–O sipinels powder without any binder and conductive. The detailed descriptions on the preparation of PME had been reported in Refs. [20,21]. All cell handling was performed in an

argon-filled glove box. Lithium was used as both the negative electrode and the reference electrode, 1 M LiPF6 dissolved in a mixture of propylene carbonate (PC) and dimethoxyethane (DME) (PC: DME = 1:1, by volume) was used as the electrolyte.

3. Results and discussion

3.1. Formation and thermo-decomposition of $LiMn(C_2O_4)(Ac)$

By grinding LiOH and oxalic acid, $LiHC_2O_4$ was synthesized as following:

$$LiOH + H_2C_2O_4 \rightarrow LiHC_2O_4 + H_2O. \quad (1)$$

The data of elemental analysis on the dried $LiHC_2O_4$ intermediate were found as C 24.84%, H 1.26%, which was well in accord with the molecular formulas ($LiHC_2O_4$ requires: C 25.03%, H 1.05%). $LiHC_2O_4$ further reacted with manganese acetate as following:

$$LiHC_2O_4 + Mn(Ac)_2 \cdot 4H_2O \rightarrow LiMnC_2O_4(Ac) + HAc + 4H_2O. \quad (2)$$

The strong vinegar odor was smelt because of the formation of acetate acid during grinding. The data of elemental analysis of the dried $LiMn(C_2O_4)(Ac)$ were found as C 23.84%, H 1.92%. Comparing with the required values ($LiMnC_4H_3O_6$ requires: C 23.00%, H 1.45%), a little high found values of C and H were resulted from the residual acetic acid molecules adsorbed on the precursor. According to the composition and synthesis principle, the structure formula of the precursor could be expressed as

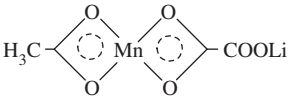

in which Mn^{2+} was coordinated respectively with the oxygen atoms of CH_3COO^- and $LiOOC–COO^-$. Accordingly, the Li^+ and Mn^{2+} were amalgamated in one precursor molecule. The IR spectrum of the precursor was shown in Fig. 2. The strong absorption bands at 1598 and 1419 cm^{-1} were attributed to the v_{as} (COO^-) and v_s (COO^-). A broad absorption band of v (O–H) was observed in range of 3700–2700 cm^{-1}. This absorption band suggested that the acetic acid molecules were adsorbed on the precursor with the hydrogen-banded mode, as was accord with the result of the elemental analysis. Three weak bands in the low-frequency region at ca. 661, 630 and 497 cm^{-1} can be respectively assigned to the v_s (Mn–O), δ (Mn–O) and v_{as} (Mn–O). It is worthwhile to note that the $LiMn(C_2O_4)(Ac)$ precursor cannot be synthesized in the solution state because it will transform into $Mn(C_2O_4)$ precipitation and LiAc solution. This kind of compounds which can only be synthesized in solid state due to the instability in the solution is called by Xin et al. as "coordination complex of weak ligand"[22,23].

Fig. 3 showed the TG and DTA curves of the precursor $LiMn(C_2O_4)(Ac)$. TG curve indicated that the weight loss occurred mainly in two steps in temperature range of 100–487 °C. In the first step, the weight loss of 7.31% was associated with the departure of methyl (Cal. 7.20%) in the temperature range of 100–190 °C, and the small exothermic peak was correspondingly observed at around 190 °C in the DTA curve. In the second step, the weight loss of 48.82% in the temperature range of 190–487 °C corresponded to the combustion of residual organic constituents (47.87%, calculated according to the $Li_2Mn_2O_4$ product) in precursor, which accompanied a strong exothermic peak at 274 °C in the DTA curve. The total weight loss in temperature range of 100–487 °C was measured as 56.13%, which was in good accord to the calculated value of 55.07% within the experimental error. These results suggested that the organic elements (C and H) in $LiMn(C_2O_4)(Ac)$ were completely decomposed in this temperature range. The detailed thermo-decomposed processes were shown in Scheme 1. The results further confirmed the structure of $LiMn(C_2O_4)(Ac)$ precursor as given above. In addition, there was a little weight loss of ab. 2% between 487 and 900 °C, which was resulted from

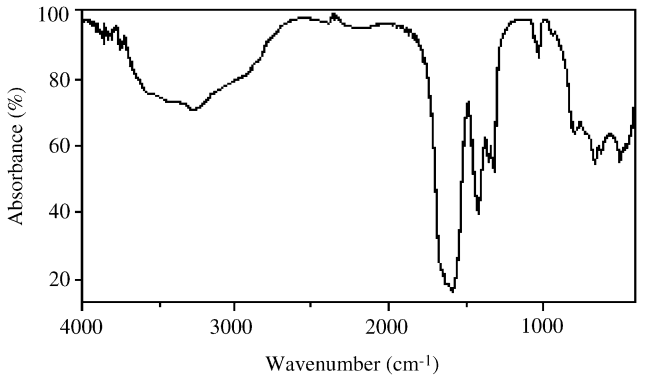

Fig. 2. IR spectrum of precursor $LiMn(C_2O_4)(Ac)$.

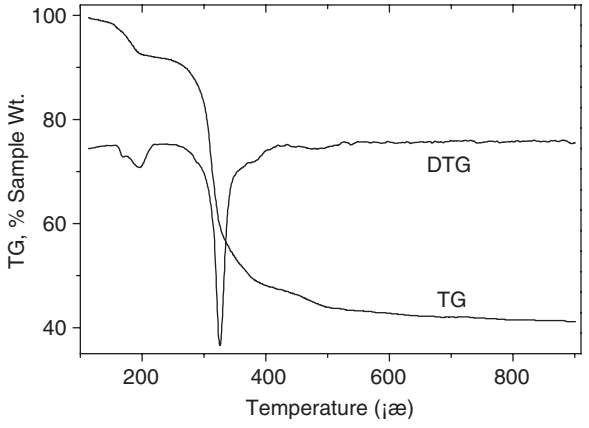

Fig. 3. TG/DTA curves of the $LiMn(C_2O_4)$ (Ac) precursor measured with a heating rate of 10 °C/min.

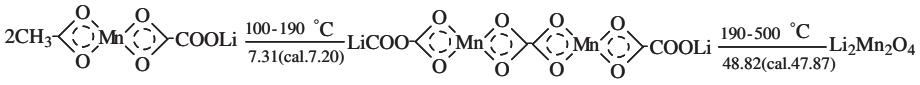

Scheme 1. Thermo-decomposition process of $LiMn(C_2O_4)(Ac)$.

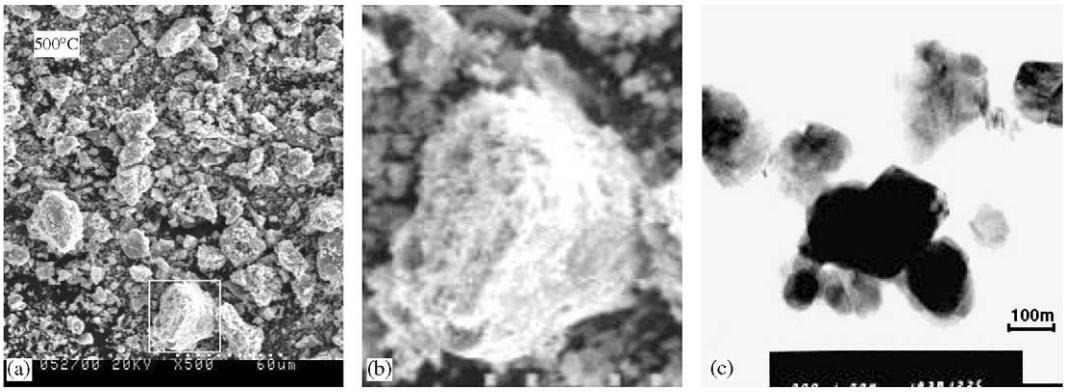

Fig. 4. The typical morphology of the powders prepared by sintering the $LiMn(C_2O_4)(Ac)$ precursor. (a) SEM micrograph of the 500 °C sample; (b) zoomed from the white pane in Fig. 3a; (c) the TEM micrograph of the 500 °C sample.

the worse stability of Li–Mn–O spinels with high Li/Mn ratio at high temperature (as seen in Section 3.2).

3.2. Morphology and phase analysis of the Li–Mn–O spinels

The morphology of all the powders prepared by sintering $LiMn(C_2O_4)(Ac)$ precursor were observed under SEM. The SEM micrographs shown in the Fig. 4 represent the typical morphological character of all the powders. Fig. 4a reveals that the powders exhibit the irregular porous agglomerates. And from Fig. 4b, it can be more clearly observed that there are many micro-holes in the surface of the particle. This porous morphology is beneficial for the diffusion of electrolyte into the interior of the particle [24], whereas is harmful to the cycleability of the Li–Mn–O cathode because the large surface area enhanced the manganese dissolution [25]. The formation of porous morphology is attributed to the escape of the gas such as CO_2 and H_2O from the interior of the particles during heat treatment. In other words, the organic constituents in $LiMn(C_2O_4)(Ac)$ precursor has bubbling effect. TEM micrograph the Fig. 4c shows that the individual crystallites are plate-like with the dimension of ca. 100 nm × 100 nm × 30 nm.

Fig. 5 showed the powder XRD patterns of the Li–Mn–O samples prepared by sintering the $LiMn(C_2O_4)(Ac)$ precursor at 450, 500, 550, 600, 700 and 850 °C. By comparing the sharpness and height of the main reflection peaks, it was clear that the sample prepared at higher sintering temperature had the better crystallinity. According to the typical XRD patterns of the various Li–Mn–O compounds summerized by Julien and Massot [26], except for the marked peaks indicating the corresponding impurities, the mainly diffraction peaks can be indexed by the cubic spinel unit cell (*Fd3m*). For the 450 °C sample, a small amount of the orthorhombic $LiMnO_2$

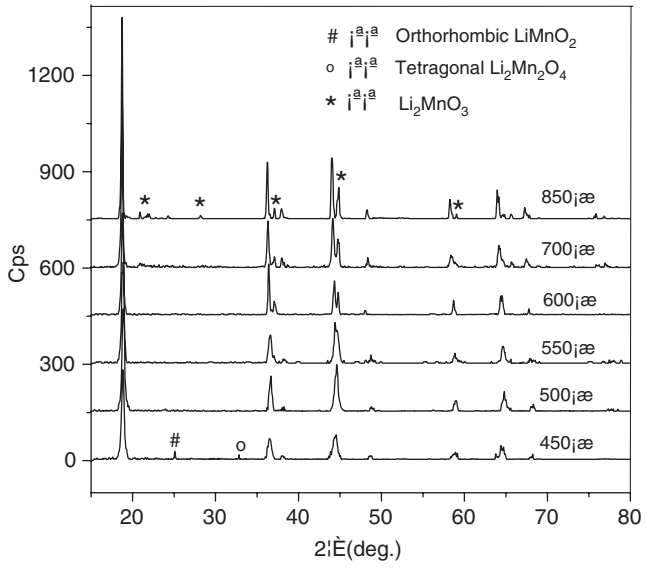

Fig. 5. XRD patterns of the Li–Mn–O spinel prepared by sintering the precursor at various temperatures for 12 h in air.

(*Pmmn*) and tetragonal $Li_2Mn_2O_4$ ($F4_1/ddm$) can be respectively observed from the diffraction peaks at $2\theta = 25.10^\circ$ (marked by #) and at $2\theta = 32.76^\circ$ (marked by °) [11,26]. When the sintering temperature increased to 500 °C, the orthorhombic $LiMnO_2$ impure phase disappeared, whereas the rock salt Li_2MnO_3 impurities ($C2/m$, especially at ab. $2\theta = 37.10^\circ$ and 44.80°, marked by ∗) emerged when the sintering temperature was above 550 °C [12,13,26]. Considering 1:1 Li/Mn ratio in the $LiMn(C_2O_4)(Ac)$ precursor, we judged that the 450 °C sample mainly consisted of the lithiated-spinel $Li_2Mn_2O_4$. However, for $Li_{1+y}[Mn_{2-x}Li_x]_{16d}O_4$ spinel series with high Li/Mn ratio, the similar oxygen array even if the different

molar fraction and different occupied site fraction (8*a*, 16*c* or 16*d*) of lithium, made them difficult to be identified distinctly by the closely similar XRD patterns [26], especially at the disturbance of the phase of Li_2MnO_3 impurities. As reported by several authors [6,13,19,26–29], the cell parameters and the electrochemical properties have

Table 1
Data of the cell parameters and potential of Li^+ intercalation/deintercalation for some stoichiometric Li–Mn–O compounds

Compounds	Structure	Cell parameters (Å)	Potential of Li^+ intercalation/deintercalation (V vs. Li^+/Li)
$LiMn_2O_4$ [21,26,29]	Cubic	$a = 8.245$	3.9/4.0, 4.05/4.15, two redox couples
$Li_4Mn_5O_{12}$ [13,26]	Cubic	$a = 8.137$	2.8/3.5, one redox couple
$Li_2Mn_2O_4$ [6,26]	Tetragonal	$a = 7.994$, $c = 9.329$	2.5/3.0, 3.9/4.0, 4.05/4.15, three redox couples
o-$LiMnO_2$ [26,28]	Orthorhombic	$a = 2.806$, $b = 5.750$, $c = 4.593$	2.5/3.0, one redox couple[a]
Li_2MnO_3 [27]	Monoclinic	$a = 8.12$[b]	3/3.5, one redox couple

[a]Transformation into spinel during cycle leads to the potentials in 4 V region.
[b]Calculated from cubic settings.

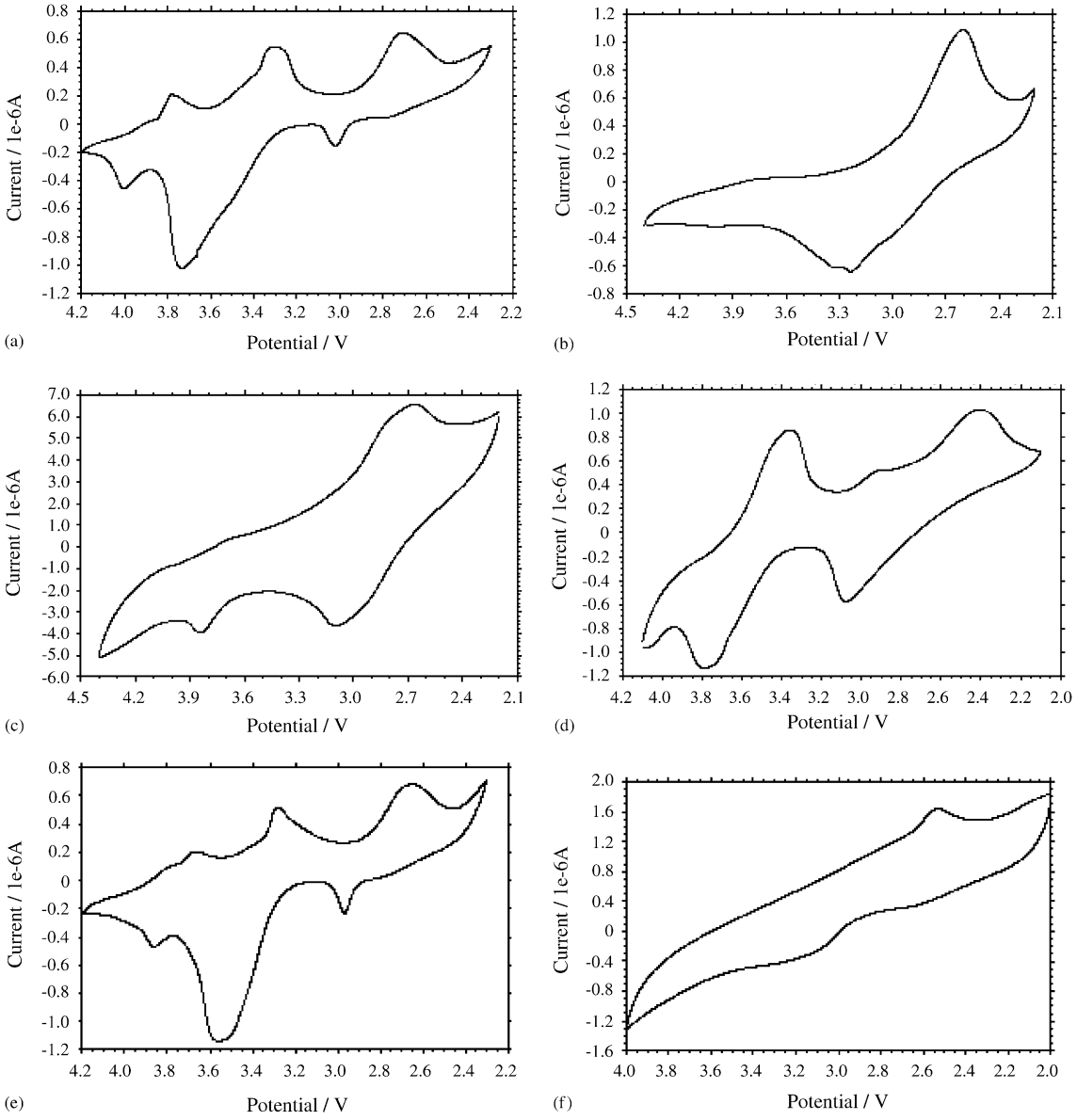

Fig. 6. CV curves of the Li–Mn–O spinels prepared by sintering the precursor at various temperatures: (a) 450 °C; (b) 500 °C; (c) 550 °C; (d) 600 °C; (e) 700 °C; (f) 850 °C.

Table 2
Cell parameters, potential of Li^+ intercalation/deintercalation and average oxidation state of Mn for the Li–Mn–O samples obtained at different sintering temperatures

Sintering temp. (°C)	Cell parameters (Å)	Potential of Li^+ intercalation/deintercalation (V vs. Li^+/Li)	Average oxidation state of Mn
450	8.163 ($a = 8.146$, $c = 8.480$)[a]	2.68/3.01, 3.30/3.72, 3.76/4.04	3.12
500	8.137	2.60/3.21	3.67
550	8.131	3.10/2.68, 3.82/3.68	3.71
600	8.187	3.78/3.36, 3.06/2.9, 2.42	3.64
700	8.203	3.86/3.66, 3.56/3.28, 2.97/2.65	3.59
850	8.216	3.21/2.53	3.52

[a]Calculated with reference to the tetrahedral unit cell.

Table 3
Structure properties of the Li–Mn–O samples obtained at different sintering temperatures

Sintering temp. (°C)	Structure of main products	Impurities
450	Cubic $Li_2Mn_2O_4$, with sightly tetragonal distortion	o-$LiMnO_2$
		Tetragonal $Li_2Mn_2O_4$
500	Similar to $Li_4Mn_5O_{12}$	—
550	Similar to $Li_4Mn_5O_{12}$	Li_2MnO_3
600	Between $Li_4Mn_5O_{12}$ and $LiMn_2O_4$	Li_2MnO_3
700	Similar to $LiMn_2O_4$	Li_2MnO_3
850	Similar to rock-salt $LiMnO_2$	Li_2MnO_3, Mn_3O_4

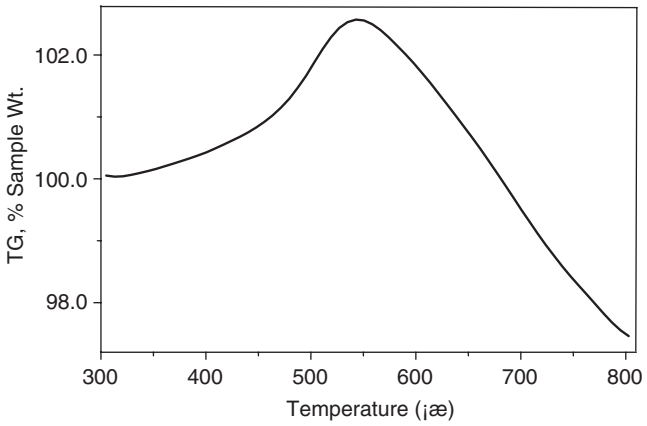

Fig. 7. TG curve of the 450 °C sample, measured with a heating rate of 10 °C/min.

more distinct differences among these $Li_{1+y}[Mn_{2-x}Li_x]_{16d}O_4$ spinel series. For some stoichiometric Li–Mn–O compounds, these differences are summarized in Table 1.

Fig. 6 shows the CV curves of the Li–Mn–O spinels obtained by sintering $LiMn(C_2O_4)(Ac)$ precursor at various temperatures. It is seen from the CV curves that the potentials of Li^+ intercalation/deintercalation (vs. Li^+/Li) have distinct difference among these Li–Mn–O samples. The data of the cell parameters (calculated from Fig. 5 with reference to the cubic spinel unit cell) and potentials of Li^+ intercalation/deintercalation for the Li–Mn–O samples obtained at different sintering temperatures are given in Table 2. It is seen that the lattice parameter decreases firstly in the sintering temperature range from 450 to 550 °C and then increases in the sintering temperature range from 550 to 850 °C. Because of the Jahn–Teller effect of Mn^{3+} in $Li_2Mn_2O_4$ for 450 °C sample, a slight distortion from cubic to tetragonal unit cell is also observed from the cell parameters ($a = 8.146$ Å, $c = 8.480$ Å, $c/a = 1.04$) calculated from the Miller indices of the tetragonal unit cell. Comparing the data of cell parameters and potential of Li^+ intercalation/deintercalation in Table 1 with that in Table 2, the phase structure of the Li–Mn–O samples obtained at different sintering temperatures can be judged as given in Table 3.

3.3. Phase transition of the Li–Mn–O spinels with high Li/Mn ratio

From the XRD patterns in Fig. 5, the intensities of diffraction peaks of Li_2MnO_3 increased clearly with raising the sintering temperature, which indicated that the content of Li_2MnO_3 in the Li–Mn–O spinels was on the increase with the sintering temperature. Clearly, the formation of Li_2MnO_3 impurities must lead to the variation of the composition of the Li–Mn–O samples because the Li/Mn ratio for Li_2MnO_3 is as twice times as the nominal Li/Mn ratio in the $LiMn(C_2O_4)(Ac)$ precursor, and consequently lead to the phase transition of the Li–Mn–O spinels. Fig. 7 showed the TG curve of $Li_2Mn_2O_4$ (450 °C sample) in the heating temperature range from 300 to 850 °C. It was observed that the mass increased gradually between 320 and 540 °C with ca. 2.41% increment. Because of the instability of the lithiated-spinel $Li_2Mn_2O_4$ at high temperature resulted from the Jahn–Teller distortion, it decomposed under the oxidizing conditions of an air atmosphere. However, the mass loss between 540 and 850 °C as shown in Fig. 6 indicated a more complicated phase transition process.

3.3.1. Phase transition in 300–550 °C

According to the formation of the Li_2MnO_3 impurities, the reaction equation can be expressed as

$$(3-3x-y)/2Li_2Mn_2O_4+(1-y)/2O_2 \rightarrow Li_{1+y}[Mn_{2-x}Li_x]_{16d}O_4+(1-2x-y)Li_2MnO_3 \quad (3)$$

x is the fraction of Li^+ occupied in the octahedral 16*d* sites, and y is the fraction of Li^+ occupied in octahedral 16*c* sites. Here, $Li_{1+y}[Mn_{2-x}Li_x]_{16d}O_4$ formula is based on the fact for the high Li/Mn ratio spinels: (i) the 8*a* tetrahedral site is fully occupied by Li [17]; (ii) except 8*a*-occupation Li, the partial extra Li (x) can substitute Mn in the octahedral 16*d* sites to form the manganese-absent spinels, typically for example as $Li_4Mn_5O_{12}$; (iii) the partial extra Li (y) can also occupy the octahedral 16*c* sites to form the lithium-rich spinels [30,31], typically for example as $Li_2Mn_2O_4$. From Eq. (3), the uptake oxygen leads to the increase of mass, as is confirmed by the TG curve in Fig. 6. According to Eq. (3), we here consider two cases as follows.

(i) For the case of "$2x+y=1$". In this case, Li_2MnO_3 phase has not formed. The oxidization of $Li_2Mn_2O_4$ is only resulted from the transfer of Li^+ from octahedral 16*c* sites to octahedral 16*d* sites. By substituted "$y=1-2x$" into Eq. (3), as a result, Eq. (3) can be expressed as:

$$(1-x/2)Li_2Mn_2O_4+xO_2 \rightarrow Li_{2-2x}[Mn_{2-x}Li_x]_{16d}O_4. \quad (4)$$

This reaction equation can also be expressed as an oxygen-rich form

$$Li_2Mn_2O_4+\delta O_2 \rightarrow Li_2Mn_2O_{4+\delta}. \quad (5)$$

Clearly, the average oxidation state of Mn in $Li_2Mn_2O_{4+\delta}$ is higher than that in $Li_2Mn_2O_4$, but the Li/Mn ratio is not varied. With the value of x increasing, $Li_2Mn_2O_4$ can be oxidized and gradually transited to a middle-phase similar to stoichiometric $Li_4Mn_5O_{12}$. As shown in Table 3, the 500 °C sample should be categorized to this case. Because the average oxidation state of Mn is increased, the thermal stability of $Li_{2-2x}[Mn_{2-x}Li_x]_{16d}O_4$ is improved. According to Eq. (4), the average oxidation state of Mn, n, can be expressed as

$$n=\frac{8}{2-x}-1 \quad (0\leqslant x\leqslant 0.333) \quad (6)$$

or

$$x=2-(8/(n+1)) \qquad y=16/(n+1)-3 \qquad (3\leqslant n\leqslant 3.8). \quad (7)$$

Fig. 8 shows the functions of $x\sim n$ and $y\sim n$ for this case. Therefore, the fraction of Li^+ in the octahedral 16*d* sites can be calculated from the average oxidation state of Mn. For $Li_2Mn_2O_4$ ($x=0$, $y=1$) in which lithium-ions occupy respectively in the tetrahedral 8*a* sites and octahedral 16*c* sites, n is +3. In the case of $x=0.333$, $Li_{2-2x}[Mn_{2-x}Li_x]_{16d}O_4$ exhibits the ideal lithium-rich $Li_{4+y}Mn_5O_{12}$ phase ($y=1$). The maximal value of n could reach +3.8 if the ratio of Li/Mn in $Li_{2-2x}[Mn_{2-x}Li_x]_{16d}O_4$ would retain at 1:1 until $x=0.333$. For examples of 450 °C sample and 500 °C sample, the XRD data in Fig. 5 suggest the Li_2MnO_3 phase has not clearly formed. From their average oxidation state of Mn as given in Table 2, we can estimate that the x fraction of Li^+ in the octahedral 16*d* sites is ab. 0.06 for 450 °C sample and 0.287 for 500 °C.

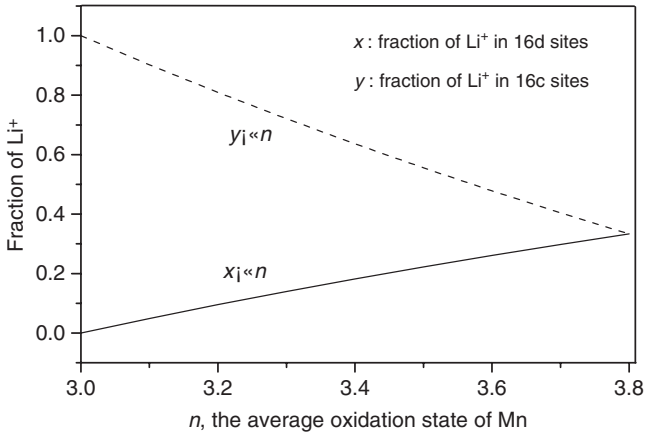

Fig. 8. Function of the average oxidation state of Mn with the fraction of Li^+ in the octahedral 16*d* sites ($x\sim n$) and octahedral 16*c* sites ($y\sim n$) for $Li_{1+y}[Mn_{2-x}Li_x]_{16d}O_4$ spinels (Li:Mn = 1, in case of $2x+y=1$).

(ii) For the case of "$2x+y\leqslant 1$". In this case, Li_2MnO_3 phase has formed. The reaction as Eq. (3) increases the average oxidation state of Mn and also lowers the Li/Mn ratio in the $Li_{1+y}[Mn_{2-x}Li_x]_{16d}O_4$ spinel phase. As a result, the thermal stability of $Li_{1+y}[Mn_{2-x}Li_x]_{16d}O_4$ spinel is further enhanced with the separation of the more stable Li_2MnO_3. According to the structure properties in Table 3, the 550 °C samples should be approximately categorized to this case. From Eq. (3), the average oxidation state of Mn in the multiphase of $Li_{1+y}[Mn_{2-x}Li_x]_{16d}O_4$ and Li_2MnO_3 can be expressed as

$$n=\frac{11-9x-5y}{3-3x-y} \quad (0\leqslant x\leqslant 0.333). \quad (8)$$

Assuming the molar ratio of $Li_{1+y}[Mn_{2-x}Li_x]_{16d}O_4$ spinel to Li_2MnO_3 phase is m, from Eq. (3), the value of m can be expressed as

$$m=1-2x-y. \quad (9)$$

Substituting Eq. (9) into Eq. (8), the fractions of Li^+ in 16*d* sites and 16*c* sites can be respectively calculated from

$$x=\frac{mn+2n-5m-6}{n+1},$$

$$y=\frac{-3mn-3n+9m+13}{n+1}. \quad (10)$$

In case if $m = 0$, i.e., Li_2MnO_3 phase has not formed, Eq. (10) just is identical with Eq. (7). From Eq. (10), theoretically, the structural properties (such as phase composition, fraction of Li^+ occupied different sites) of $Li_{1+y}[Mn_{2-x}Li_x]_{16d}O_4$ spinel can be quantitatively analyzed by the data of XRD and average oxidation state of Mn. In fact, the value of m is not easy to be accurately determined only by the XRD data because of two factors. Firstly, the main diffraction peaks of the rock salt Li_2MnO_3 are overlapped with those of $Li_{1+y}[Mn_{2-x}Li_x]_{16d}O_4$ phase. Secondly, the upgrowth degree of Li_2MnO_3 phase toward different crystal face has some difference during formation of Li_2MnO_3 phase. The detail for this complex case will be separately discussed in the other paper.

It is worth to note that the Li_2MnO_3 phase begins to form even if the value of x does not reach 0.333. For 550 °C sample, assuming that the content of Li_2MnO_3 phase is zero ($m = 0$), from its average oxidation state of Mn (+3.71), the value of x also is only 0.301. Therefore, during the transfer of Li^+ from octahedral 16*c* sites to octahedral 16*d* sites, there is a competition between the individual $Li_2Mn_2O_{4+\delta}$ phase ($2x + y = 1$) and the formation of Li_2MnO_3 phase ($2x + y \leqslant 1$). Consequently, both of the ideal tetragonal $Li_2Mn_2O_4$ ($x = 0$, $y = 1$) and ideal $Li_{4+\delta}Mn_5O_{12}$ phase ($x = 0.333$) are difficult to be obtained.

3.3.2. Phase transition in 550–850 °C

In this temperature range, the TG curve in Fig. 7 shows a mass-decreasing process. Note that $Li_{1+y}[Mn_{2-x}Li_x]_{16d}O_4$ spinel at ab. 500 °C has exhibited the stoichiometric $Li_4Mn_5O_{12}$-like structure as discussed above. As suggested by Thackeray et al. [12,32,33], the stoichiometric $Li_4Mn_5O_{12}$ would decompose to the more stable $LiMn_2O_4$ and Li_2MnO_3 at temperatures higher than 400 °C, which is associated with the evacuation of oxygen as following:

$$Li_4Mn_5O_{12} \rightarrow 2LiMn_2O_4 + Li_2MnO_3 + 1/2O_2. \quad (11)$$

When the sintering temperature is above 900 °C, the rock-salt $LiMnO_2$ phase can be formed by the reaction between $LiMn_2O_4$ and Li_2MnO_3:

$$LiMn_2O_4 + Li_2MnO_3 \rightarrow 3LiMnO_2 + 1/2O_2. \quad (12)$$

From the CV curve of 550 °C sample in Fig. 6c, a small redox couple at 3.82 V/3.68 V indicates the a little transition from stoichiometric $Li_4Mn_5O_{12}$-like structure to $LiMn_2O_4$-like structure. For the 700 °C sample, a large redox couple at 3.86 V/3.66 V in Fig. 6e suggests that $Li_{1+y}[Mn_{2-x}Li_x]_{16d}O_4$ spinel with $LiMn_2O_4$-like structure has been largely formed. Because the potential of Li^+ intercalation/deintercalation in the 4 V region is not observed among the 550–700 °C samples, the structure of the these samples are in the middle-phase between $Li_4Mn_5O_{12}$ and $LiMn_2O_4$. In this temperature range, lithium-ions gradually break away from the octahedral 16*d* sites to form the Li_2MnO_3 phase, which makes the value of x gradually decreasing and the content of Li_2MnO_3 phase further increasing. Consequently, the average oxidation state of Mn also decreases with the evacuation of oxygen as shown in Table 2. However, from the CV curve of the 850 °C sample in Fig. 6f, only a weak redox couple at 3.21 V/2.53 V is observed, which indicates a phase transition from $LiMn_2O_4$ phase to the rock-salt $LiMnO_2$ phase of which the electrochemical activity is very poor. These results confirm that the reactions as given in Eqs. (11) and (12) are also applicable to $Li_{1+y}[Mn_{2-x}Li_x]_{16d}O_4$ with the non-stoichiometric $Li_4Mn_5O_{12}$-like structure.

3.3.3. Brief summary and kinetic expectation

According to above discussion, the phase transition of Li–Mn–O spinel with high ratio of Li/Mn was outlined as shown in Fig. 9. Here, we emphasize that the transfer of Li^+ from 16*c* sites to 16*d* sites play a very important role in the phase transition of Li–Mn–O spinels with the high

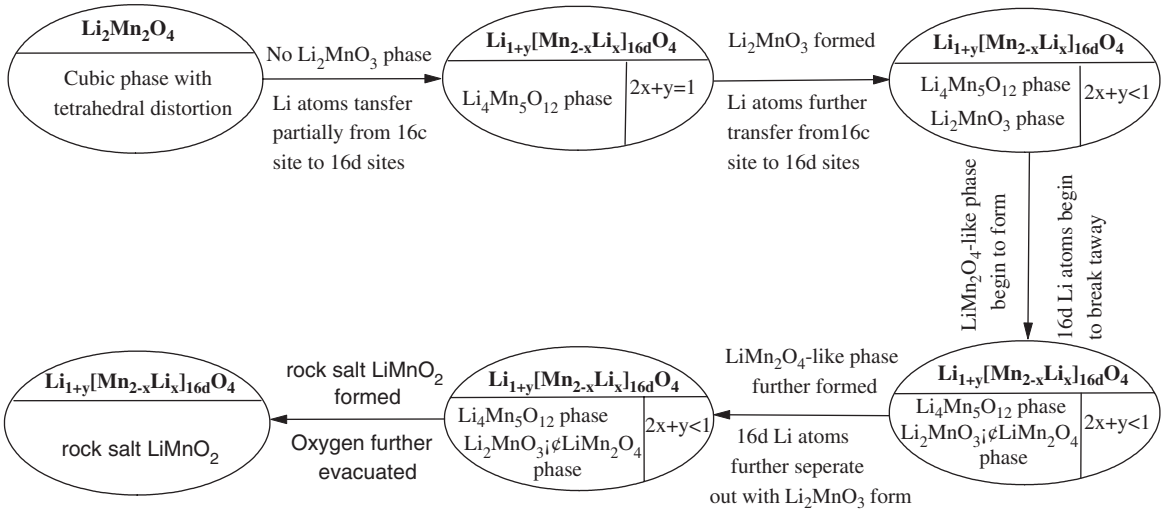

Fig. 9. Schematic illumination on the phase transition mechanism of Li–Mn–O spinels with 1:1 Li/Mn ratio.

Li/Mn ratio. The neutron diffraction studies had confirmed the manganese vacancies in 16*d* sites were partially occupied by Li^+ [30,34,35]. From the view of the thermodynamics, Gao et al. [36–38] proposed the most stable structure of 16*d* Li^+ in $Li_y[Mn_{2-x}Li_x]_{16d}O_4$ was that three lithium-ions were pinned around one 16*d* lithium-ion. Therefore, the transfer of Li^+ from 16*c* sites to 16*d* sites not only frustrated the ordering reaction in $Li_{1+y}[Mn_{2-x}Li_x]_{16d}O_4$ but also weakened the link between 4.0 and 4.15 V plateaus. This was consistent with above discussion that the value of x is very sensitive to the sintering temperature and the potential of Li^+ intercalation/deintercalation. However, the kinetics of the transfer of Li^+ from 16*c* sites to 16*d* sites has not been better understood. From this study, we can confirm a kinetic competition between the transfer of Li^+ from 16*c* sites to 16*d* sites to increase the Li^+ content in 16*d* sites and the formation of Li_2MnO_3 phase to decrease the Li^+ content in 16*d* sites. At higher concentration of Li^+ in 16*d* sites and higher sintering temperature, the kinetic competition would be in favor of the formation of Li_2MnO_3 phase. Considering a simple description for this kinetic competition:

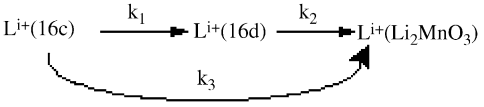

(13)

the kinetic equation for $Li_{1+y}[Mn_{2-x}Li_x]_{16d}O_4$ can be expressed as

$$\frac{dx}{dt} = k_1 y - k_2 x,$$
$$\frac{dy}{dt} = -(k_1 + k_3) y. \quad (14)$$

Because the composition of the spinel $Li_{1+y}[Mn_{2-x}Li_x]_{16d}O_4$ electrode play a very important role in controlling the electrochemical properties of the electrode [35,39], the control of synthesis process to obtain the spinel $Li_{1+y}[Mn_{2-x}Li_x]_{16d}O_4$ materials with required composition and structure must understand the kinetic properties of synthesis process.

4. Conclusions

A new process for the synthesis of the meta-stable $Li_{1+y}[Mn_{2-x}Li_x]_{16d}O_4$ spinels with high ratio of Li/Mn was developed on the Mn^{2+} and Li^+ high-ordered LiMn C_2O_4(Ac) precursor by the room-temperature solid-state reaction. The composition, structure and electrochemical properties of obtained $Li_{1+y}[Mn_{2-x}Li_x]_{16d}O_4$ samples were very sensitive to the sintering temperature of the precursor. The sample obtained at 450 °C mainly exhibited the structure of lithiated-spinel $Li_2Mn_2O_4$ with a slight tetragonal distortion. With the sintering temperature increasing, the phase transition occurred. By XRD, CV curve and average oxidation state of Mn, the phase transition process of the $Li_{1+y}[Mn_{2-x}Li_x]_{16dt}O_4$ spinels with high Li/Mn ratio had been investigated. Results showed that the transfer of Li^+ from 16*c* sites to 16*d* sites played a very important role in the phase transition of Li–Mn–O spinels. In addition, a way of determining x in the $Li_{1+y}[Mn_{2-x}Li_x]_{16d}O_4$ spinel with average oxidation state of Mn and the content of Li_2MnO_3 was also demonstrated.

Acknowledgments

This work was supported by NNSF of China (No.20406024) and the Postdoctoral Science Foundation of Central South University (No.76600).

References

[1] M.M. Thackeray, J. Am. Ceram. Soc. 82 (1999) 3347–3354.
[2] B. Goodenough, M.M. Thackeray, W.I.F. David, P.G. Bruce, Rev. Chim. Miner. 21 (1984) 435–455.
[3] D. Zhang, B.N. Popov, R.E. White, J. Power Sources 76 (1998) 81–90.
[4] H.J. Bang, V.S. Donepudi, J. Prakash, Electrochim. Acta 48 (2002) 443–451.
[5] A.D. Robertson, S.H. Lu, W.F. Averill, W.F. Howard Jr., J. Electrochem. Soc. 145 (4) (1998) 1131–1136.
[6] D. Peramunage, K.M. Abraham, J. Electrochem. Soc. 145 (4) (1998) 1131–1136.
[7] P. Endres, B. Fuchs, S. Kemmler-Sack, K. Brandt, G. Faust-Becker, H.-W. Praas, Solid State Ionics 89 (1996) 221–231.
[8] A. Ott, P. Endres, V. Klein, B. Fuchs, A. Jager, H.A. Mayer, S. Kemmler-Sack, H.-W. Praas, K. Brandt, G. Filot, V. Kunczer, M. Rosenberg, J. Power Sources 72 (1998) 1–8.
[9] A.I. Polos, A. Anne, P. Strobel, J. Solid State Chem. 160 (2001) 108–117.
[10] A. Blyr, C. Sigala, G. Amatucci, D. Uyomard, Y. Chabre, J.-M. Tarascon, J. Electrochem. Soc. 145 (1) (1998) 194–209.
[11] R.J. Gummow, D.C. Liles, M.M. Thackeray, Mater. Res. Bull. 28 (1993) 1249–1256.
[12] M.M. Thackeray, M.F. Mansuetto, C.S. Johnson, J. Solid State Chem. 125 (1996) 274–277.
[13] T. Takada, H. Hayakawa, E. Akiba, J. Solid State Chem. 115 (1995) 420–426.
[14] Y.C. Zhang, H. Wang, B. Wang, H. Yan, A. Ahniyaz, M. Yoshimura, Mater. Res. Bull. 37 (2002) 1411–1417.
[15] A. Ibarra Palos, M. Anne, P. Strobel, J. Solid State Chem. 160 (2001) 108–117.
[16] Y. Xia, T. Sakai, T. Fujieda, X.Q. Yang, X. Sun, Z.F. Ma, J. Mcbreen, M. Yoshio, J. Electrochem. Soc. 148 (7) (2001) A723–A729.
[17] M. Yonemura, A. Yamada, H. Kobayashi, M. Tabuchi, T. Kamiyama, Y. Kawamoto, R. Kanno, J. Mater. Chem. 14 (2004) 1948–1958.
[18] X.-C. Tang, L.-P. He, Z.-Z. Chen, D.-Z. Jia, X. Xia, Chem. J. Chin. Univ. 24 (4) (2003) 576–579.
[19] Y. Huang, J. Li, D. Jia, J. Colliod Interface Sci. 286 (2005) 263–267.
[20] P.F. Liu, C.S. Cha, X. Li, J. Chen, Chem. J. Chin. Univ. 15 (1994) 725–729.
[21] C.S. Cha, C.M. Li, H.X. Yang, P.F. Liu, J. Electroanal. Chem. 68 (1994) 47–53.
[22] J.X. Chen, T. Pan, M.G. Liu, S.F. Lin, X.Q. Xin, Acta Chim. Chin. 60 (1) (2002) 60–64.
[23] Y.M. Zhou, X.Q. Xin, Chin. J. Inorg. Chem. 15 (3) (1999) 273–292.
[24] X.C. Tang, L.P. He, Z.Z. Chen, D.Z. Jia, Chin. J. Inorg. Chem. 18 (6) (2002) 591–596.

[25] X.C. Tang, Y.P. Yang, L.Q. Li, D.Z. Jia, K.L. Huang, Chin. J. Nonferr. Met. 14 (5) (2004) 871–876.
[26] C.M. Julien, M. Massot, Mater. Sci. Eng. B 100 (2003) 69–78.
[27] P. Kalyani, S. Chitra, T. Mohan, S. Gopukumar, J. Power Sources 80 (1999) 103–106.
[28] Y.S. Lee, M. Yoshio, Electrochem. Solid-State Lett. 4 (10) (2001) A166–A169.
[29] T. Takada, H. Enoki, H. Hayakawa, E. Akiba, J. Solid State Chem. 139 (1998) 290–298.
[30] H. Berg, E.M. Kelder, J.O. Thomas, J. Mater. Chem. 9 (1999) 427–429.
[31] H. Berg, K. Goransson, B. Nolang, J.O. Thomas, J. Mater. Chem. 9 (1999) 2813–2820.
[32] A. Riou, A. Lecerf, Y. Gerault, Y. Cudennec, Mater. Res. Bull. 27 (1992) 269–275.
[33] M.M. Thackeray, M.F. Mansuetto, D.W. Dees, D.R. Vissers, Mater. Res. Bull. 31 (2) (1996) 133–140.
[34] B. Ammundsen, D.J. Jones, J. Rozière, Chem. Mater. 10 (1998) 1680–1687.
[35] T. Takada, E. Akiba, F. Izumi, B.C. Chakoumakos, J. Solid State Chem. 130 (1997) 74–80.
[36] Y. Gao, M.N. Richard, J.R. Dahn, J. Appl. Phys. 80 (1996) 4141–4152.
[37] Y. Gao, J.R. Dahn, J. Electrochem. Soc. 143 (1) (1996) 100–114.
[38] R. Darling, J. Newman, J. Electrochem. Soc. 146 (10) (1999) 3765–3772.
[39] R.J. Gummow, A. De Kock, M.M. Thackeray, Solid State Ions 69 (1994) 59–67.